Anomaly, class division, and decoupling in income dynamics

Jaeseok Hur [1], Meesoon Ha [2,*] and Hawoong Jeong [1,3,†]
[1]*Department of Physics, Korea Advanced Institute of Science and Technology, Daejeon 34141, Korea*
[2]*Department of Physics Education, Chosun University, Gwangju 61452, Korea*
[3]*Center of Complex Systems, KAIST, Daejeon 34141, Korea*

(Received 9 June 2025; revised 29 November 2025; accepted 22 April 2026; published 12 May 2026)

Economic inequality emerges from the interplay between regional growth-rate differences and the interaction network that couples regions. We propose a minimal income-dynamics model, where heterogeneity is governed by growth-rate assortativity $\mathcal{A}$ and regional concentration $\mathcal{R}$, allowing us to quantify the spatiotemporal patterns of empirically observed log-income distributions. To systematically analyze these patterns, we derive closed-form approximations for the Hellinger distance and the Gini index in limiting configurations. Our findings highlight the spatial segregation of growth rates as a key driver of economic class division and demonstrate how small-world shortcuts in the underlying network can disrupt this segregation. Finally, our framework provides a robust explanation for the bimodality and strong regional correlations found in global income distributions.

DOI: 10.1103/66j8-zpyg

I. INTRODUCTION

Since the publication of Piketty's *Capital in the Twenty-first Century* [1] ignited a debate on the mechanism of economic inequality, both wealth and income distributions have been widely addressed in both theoretical [2–8] and empirical studies [9–20]. In *World Inequality Report 2022* [21], global income inequality for the period 1950–2010 was attributed to regional location [10,11]. Such inequality, as represented by the Gini index, peaked in the late twentieth century, and income distributions were bimodal. Strong regional correlations were observed in the global income levels of countries [22], and the corresponding regional convergence was studied in [23,24].

The most recent study by Milanovic [12] divided the history of global-income inequality into three eras: In the first era, both within and between inequality increases, characterized by persistently increasing segregation of income levels. In the second era, high global inequality and regional segregation become chronic, characterized by the bimodality of income distributions. In the third era, corresponding to the contemporary era, it no longer exhibits any bimodality in income distributions, caused by the acceleration of growth rates in developing countries, such as China and India [12–14].

In this paper we provide a comprehensive picture of inequality in the first two eras of [12], where spatiotemporal patterns of income dynamics exhibit bimodality (class division between the rich and the poor) and regional segregation (location dependence) of income levels [11]. We address fundamental questions in economic inequality: how can such a mechanism be formulated, in the context of a prototype pedagogical model, and what are the key ingredients of such a model? Modeling income dynamics as a binary mixture of growth rates, which is analogous to quenched disorder in physical systems, we implement both class division and decoupling of two growth rate groups. Our hypothesis is that bimodality and regional segregation of income levels are driven by heterogeneity of growth rates and low connectivity between regions with different growth rates. Hence, the model is tested in a one-dimensional (1D) ring analytically and in a sparse regular and small-world (SW) network numerically.

Our model can be considered as the heterogeneous case of the wealth-dynamics model by Bouchaud and Mézard (BM) [25], in which the configuration of binary growth rates is tuned by regional growth rate assortativity $\mathcal{A}$ and concentration $\mathcal{R}$ (see Fig. 1). For the homogeneous case, we provide rigorous analytical derivations and more detailed results in Appendix A and Sec. I in the Supplemental Material (SM) [26].

Since the allocation of binary growth rates influences the spatiotemporal patterns of income dynamics, we unveil the conditions under which bimodal income distributions can be observed. In a 1D ring, a slowly decaying field exponent η produces subdiffusive broadening of log-income within groups, while configuration governs structure: $\mathcal{R}$ drives decoupling and bimodality, and $\mathcal{A}$ sets the pace of inequality growth. Closed-form approximations for the Hellinger distance h and the Gini index g quantify these effects. Adding SW shortcuts weakens long-range correlations, disrupts segregation, and collapses bimodality, identifying spatial segregation, not growth rate differences alone, as a key mechanism of class division. Finally, we conclude with a comprehensive picture of global income inequality and a possible remedy to alleviate it.

II. MODEL

We introduce a binary mixture of growth rates into the BM model on a network topology. The following stochastic differential equation (SDE) is for the heterogeneous BM

*Contact author: msha@chosun.ac.kr
†Contact author: hjeong@kaist.edu

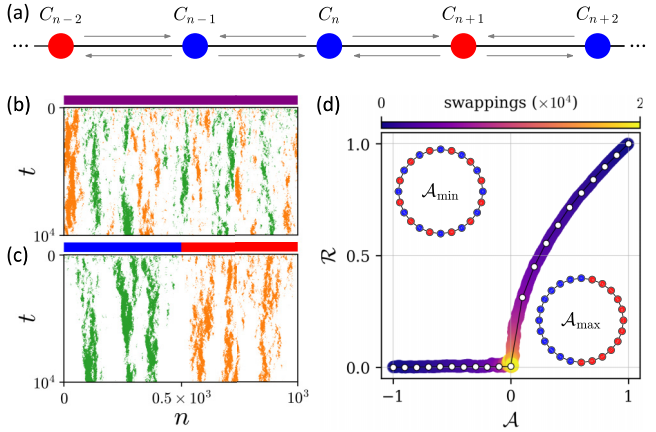

FIG. 1. (a) Schematic illustration of income dynamics with a binary mixture of regional growth rate in the HBM model: • (α_+, red) and • (α_-, blue) for $\alpha_\pm = \alpha \pm \Delta\alpha$ and income (C) transfer (either $\rightarrow$ or $\leftarrow$) between two nearest-neighboring sites. (b), (c) Snapshots of spatiotemporal patterns for a top-rich/bottom-poor 10% (orange/green) class are taken from a single run for two extreme configurations: ($\mathcal{A}_{\min}$, $\mathcal{A}_{\max}$): The position index n is shown in horizontal from left to right, and time t is in vertical from top to bottom. Here $N = 10^3$, $\alpha = 10^{-2}$, $\Delta\alpha = 10^{-3}$, $\beta^2 = 10^{-3}$, and $J = 10^{-1}$ in Eq. (1). (d) Random pair swapping trajectories of ($\mathcal{A}$, $\mathcal{R}$). A path starts from two extreme configurations with ($\mathcal{A}_{\min/\max}$, $\mathcal{R}_{\min/\max}$) (see insets). Each random pair-swapping trial is represented by color gradation. The interval of simulation samples (○) is 0.1 in $[\mathcal{A}_{\min}, \mathcal{A}_{\max}]$.

(HBM) model [see Fig. 1(a)]:

$$dC_n = \alpha_n C_n dt + \beta C_n dW_{t,n} + J\left(\bar{C}_n^{(k)} - C_n\right)dt, \qquad (1)$$

where C_n is the income at a node n, dt is a time interval, $W_{t,n}$ is the Wiener process at n at time t, $\alpha_n = \alpha \pm \Delta\alpha$ is the growth rate at n, β is volatility, J is the strength of interaction between two coupled neighbors, and $\bar{C}_n^{(k)}$ is the average income for k neighbors at n, respectively. Initially, all nodes have the same income. This SDE follows the Itô interpretation. We note that both α and $\Delta\alpha$ are positive constants, preserving $\alpha > \Delta\alpha$.

Since the SDE [Eq. (1)] incorporates quenched disorder, the growth-rate configuration remains static. The disorder of the growth rate configuration disrupts the translational invariance of the system. The transformation analysis of the ordinary BM model cannot hold.

Without loss of generality, we consider the case that the number of nodes for the group of α_+ is the same as that of α_-: $N_+ = N_-$ and $\alpha_\pm = \alpha \pm \Delta\alpha$ [see Figs. 1(b) and 1(c) for two extreme configurations]. In Fig. 1(b) the alternative allocation generates the spatiotemporal patterns of top-rich (orange)/bottom-poor (green) 10 while in Fig. 1(c), the fully separated allocation displays regional segregation (class division) and long-range spatial correlations (clustering).

Statistical properties and control parameters

We quantify the statistical properties of the allocation of $\alpha_\pm$ and generate all possible configurations in terms of two relevant control parameters.

The first parameter of Fig. 1(d), growth-rate assortativity $\mathcal{A}$, quantifies the connectivity between regions with similar α values connected in a given network:

$$\mathcal{A} \equiv \frac{\mathrm{Cov}(\alpha, \alpha')}{\sqrt{\mathrm{Var}(\alpha)\mathrm{Var}(\alpha')}}, \qquad (2)$$

where α and α' are the growth rates in two connected regions for a given network, respectively.

For the binary mixture in the 1D ring with $N_+ = N_-$, $\mathcal{A} = \rho^{(1)} - \rho^{(2)}$, where $\rho^{(1)}$ and $\rho^{(2)}$ are homogeneous and heterogeneous link densities, respectively (see Sec. II A in SM [26] for the definition and detailed derivations). The actual bounds [27] of $\mathcal{A}$ depend on the network topology [28]. In the 1D ring, the alternative allocation of growth rates becomes the lower bound of $\mathcal{A}$, and the fully separated allocation becomes the upper bound of $\mathcal{A}$: $\mathcal{A}_{\min} = -1$ for Fig. 1(b) and $\mathcal{A}_{\max} = +1 - 4/N$ for Fig. 1(c), illustrated as the insets in Fig. 1(d).

The second parameter in Fig. 1(d), $\mathcal{R}$, is derived from the phase order parameter in the Kuramoto model [29], which represents the polar concentration of growth rates in the 1D ring. Intuitively, $\mathcal{R}$ serves as a topological metric that quantifies the spatial clustering of growth rates on the ring as well. Thus, $(r_\pm, \psi_\pm)$ is $r_\pm e^{i\psi_\pm} = \frac{1}{N_\pm}\sum_j e^{i\phi_j^{(\pm)}}$, where $\phi_j^{(\pm)}$ is the angular argument for binary growth rate groups, respectively.

In the 1D HBM model, all regions are assigned in a 1D ring with the same intervals. Thus, $\phi_j = 2\pi m/N$, where $m \in \{0, \ldots, N-1\}$. For the case of $N_+ = N_-$ and $r_\pm \neq 0$, two important quantities become $r_+ = r_- = r$ and $\Delta\psi = |\psi_+ - \psi_-| = \pi$. For any configuration, $\Delta\psi$ is either π or "not defined" ($r = 0$), so we only consider r. For the perfectly disassortative case with $\mathcal{A}_{\min}$ and the perfectly assortative case with $\mathcal{A}_{\max}$, $r \to 0$ and $r \to 2/\pi$ as $N \to \infty$, which are the minimum and the maximum, respectively (see Sec. II B and Fig. S5 in SM [26] for detailed definitions and discussions). Hence, $\mathcal{R}$ is defined as a statistical control parameter:

$$\mathcal{R} \equiv r/(2/\pi). \qquad (3)$$

III. RESULTS

To characterize spatiotemporal patterns in income distributions, we employ two standard statistical measures: Hellinger distance h [30] and Gini index g [31].

First, h is defined as

$$h(\rho_1, \rho_2) \equiv \sqrt{\frac{1}{2}\int (\sqrt{\rho_1(x)} - \sqrt{\rho_2(x)})^2 dx}, \qquad (4)$$

where $0 \leqslant h \leqslant 1$ and $\rho_i(x)$ is a probability distribution of log-normalized income x [32]. This follows the Lebesgue measure. The entire ρ can be decomposed by $\rho_{\alpha_\pm}$ (see Fig. 2), $\rho = (\rho_{\alpha_-} + \rho_{\alpha_+})/2$. Hence $h(\rho_{\alpha_-}, \rho_{\alpha_+}) = 0$ (1) is a perfectly coupled (decoupled) state (see Figs. 1 and 2).

Second, g is defined as

$$g \equiv \frac{1}{2\langle c\rangle}\int_0^\infty \int_0^\infty \rho(c)\rho(c')|c - c'|dcdc', \qquad (5)$$

where $0 \leqslant g \leqslant 1$ and $\rho(c)$ is a probability distribution of normalized income $c \equiv C/\bar{C}$. Hence, $g = 0$ (1) is the perfect equality (extreme inequality as a condensation state with the whole income monopolized by a few regions).

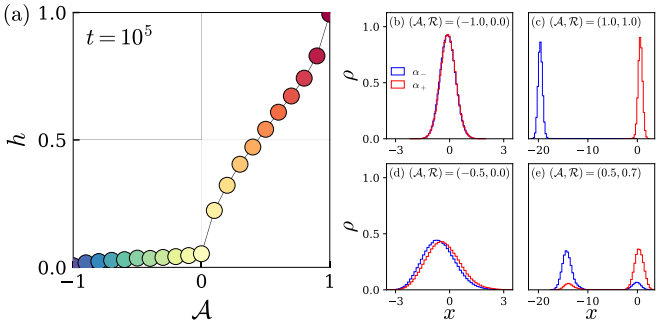

FIG. 2. Configuration effect on decoupling by Hellinger distance h: (a) h in Eq. (4) plotted at $t = 10^5$ against $\mathcal{A}$ with $\mathcal{R}(\mathcal{A})$; see Fig. 1(d). Selected snapshots for unimodal and bimodal distributions: (b), (c), (d), and (e) are the cases of $(\mathcal{A}, \mathcal{R}) = (-1.0, 0.0)$, $(-0.5, 0.0)$, $(0.5, 0.7)$, and $(1.0, 1.0)$ for $t = 10^4$, respectively. Here $N = 10^4$, results are obtained by 128 runs, and the other parameters are the same as Fig. 1.

For the sampling of growth rate configurations, we perform the random pair swapping algorithm: (1) Start from two extreme configurations, $(\mathcal{A}_{\min}, \mathcal{R}_{\min})$ and $(\mathcal{A}_{\max}, \mathcal{R}_{\max})$, respectively. (2) Select a random pair of regions and switch positions. If this process is repeated for large iterations, $(\mathcal{A}, \mathcal{R})$ almost converges to near (0,0) [see Fig. 1(d)]. To elucidate the impact of growth rate configurations of regional growth rates on income dynamics at a glance, we compare two extreme cases of the configurations, $\mathcal{A}_{\min}$ and $\mathcal{A}_{\max}$: For the perfectly disassortative case, $\rho(x, t; \mathcal{A}_{\min})$ is

$$\rho(x, t; \mathcal{A}_{\min}) \approx \rho_{\alpha_\pm}(x, t) \sim \mathcal{N}\left(\mu_t, \sigma_t^2\right), \tag{6}$$

where $\sigma_t^2 = \beta^2 t^\lambda/(2Ja_0)$, $\mu_t = -\sigma_t^2/2$ for large t, and $0.5 \leqslant \lambda \leqslant 1$. These results are consistent with the homogeneous BM model in the 1D ring topology (see Sec. I in SM [26] for detailed derivations). For the case of $h \approx 0$, $\rho_{\alpha_\pm}$ almost perfectly overlap each other [see Fig. 2(b)]. The perfectly disassortative configuration neutralizes the impact of heterogeneous growth rates on income distributions. For the perfectly assortative case, $\rho(x, t; \mathcal{A}_{\max})$ for large t is divided into three parts [see Fig. 2(c)] with two well-separated Gaussian peaks: (1) Gaussian peak around the first mode (head), $\rho^{(\mathrm{h})}$, (2) flat region between the two peaks (body), $\rho^{(\mathrm{b})}$, and (3) Gaussian peak around the second mode (tail), $\rho^{(\mathrm{t})}$:

$$\rho(x, t; \mathcal{A}_{\max}) \approx \begin{cases} \rho^{(\mathrm{h})}(x, t) & \sim \mathcal{N}\left(\mu_t^-, \sigma_t^2\right), \\ \rho^{(\mathrm{b})}(x, t) & \sim \text{const}, \\ \rho^{(\mathrm{t})}(x, t) & \sim \mathcal{N}\left(\mu_t^+, \sigma_t^2\right), \end{cases} \tag{7}$$

where $\mu_t^\pm \approx \mu_t + \ln[2/(1 + e^{\mp 2\Delta\alpha t})]$. σ_t^2 and μ_t are the same as before. $\rho^{(\mathrm{h})}$ and $\rho^{(\mathrm{t})}$ are formed by lower and higher growth rate nodes, respectively (see Sec. III and Figs. S6 and S7 in SM [26] for details).

While the motions in the same growth rate group are subdiffusive, represented by σ_t^2, the relative motion between the different groups of $\alpha_\pm$ is ballistic, represented by income level segregation that increases linearly in t, $\Delta\mu = \langle x_{\alpha+\Delta\alpha}\rangle - \langle x_{\alpha-\Delta\alpha}\rangle \approx 2\Delta\alpha t$. Since $\Delta\mu$ increases faster than σ_t, there is almost no overlap between $\rho_\pm$ for large t and it demonstrates $h \approx 1$. In other words, the perfectly assortative configuration maximizes decoupling. Surprisingly, this linearity is also

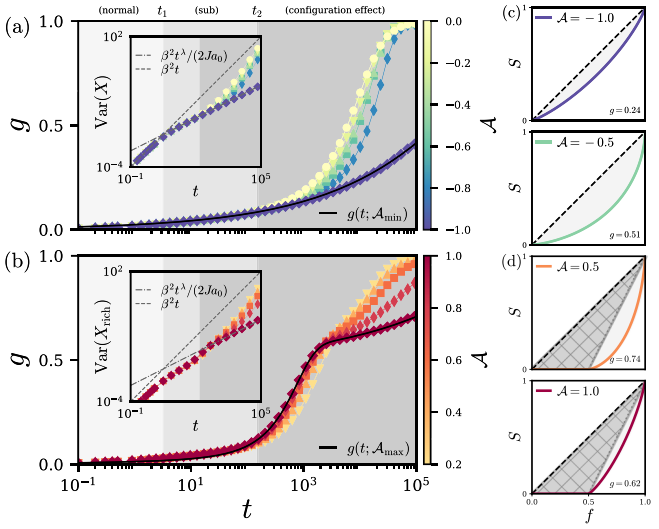

FIG. 3. Configuration effect on inequality by Gini index g against t: Each color reflects the selected samples of $\mathcal{A}$ with $\mathcal{R}$ in Fig. 1(d). *Path 1* (a) of $(\mathcal{A}_{\min}, \mathcal{R}_{\min}) \to (0, 0)$ and *Path 2* (b) of $(\mathcal{A}_{\max}, \mathcal{R}_{\max}) \to (0, 0)$, respectively. As t elapses, the system exhibits normal diffusion (below t_1), subdiffusion ($t_1 \leqslant t \leqslant t_2$) and finally reaches the configuration-effect dominant diffusion (above t_2). Insets in (a) and (b) are $\mathrm{Var}(X)$ and $\mathrm{Var}(X_{\mathrm{rich}})$, respectively, where the guided lines are drawn for normal diffusion and subdiffusion as described, respectively. Lorenz curves (c) and (d) of S against f at $t = 10^4$ correspond to Figs. 2(b)–2(d) and Figs. 2(c)–2(e), where plain and hatched shadow regions illustrate the contributions of class division and diffusion to g, respectively.

consistent for *Path 2* configurations such that $\Delta\mu \approx \mathcal{A} \times 2\Delta\alpha t$. It exhibits that configurational property $\mathcal{A}$ also controls income level segregation $\Delta\mu$ (see Sec. III and Figs. S8 and S9 in SM [26] for detailed derivations and numerical confirmations).

For the perfectly disassortative case [see Fig. 3(a)], $g(t; \mathcal{A}_{\min})$ is

$$g(t; \mathcal{A}_{\min}) \approx \mathrm{erf}(\sigma_t/2). \tag{8}$$

Increasing $g(t)$ is only driven by subdiffusion because there is almost no decoupling between $\rho_{\alpha_\pm}(x, t)$.

For the perfectly assortative case [see Fig. 3(b)], $g(t; \mathcal{A}_{\max})$ is

$$g(t; \mathcal{A}_{\max}) \approx \frac{1}{2}\left(1 - \frac{2}{1 + e^{2\Delta\alpha t}}\right) + \frac{1}{2}\mathrm{erf}(\sigma_t/2). \tag{9}$$

The first term of Eq. (9) captures the inequality between the $\alpha_\pm$ groups. It converges rapidly to $1/2$ because the regional segregation of income levels leaves the α_- group (comprising 50% of the population) with a negligible share of the total income. The second term accounts for the inequality within the α_+ group, converging gradually to $1/2$ due to the subdiffusive broadening of the Gaussian peaks shown in Fig. 2(c). Detailed derivations are provided in Appendix B and Sec. III B in SM [26]. This result serves as a compelling illustration of the dominant influence of location (region or country) [11] on income levels, highlighting the distinct contributions of between- and within-group inequalities [14] to the global system.

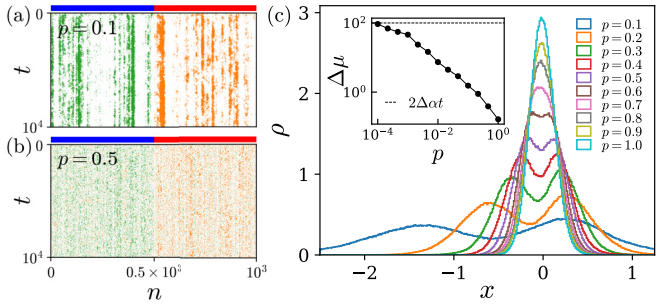

FIG. 4. SW effect on the HBM model: Spatiotemporal patterns of top-rich (orange)/bottom-poor (green) 10% classes over positional index n for a fully separated configuration with rewiring probability (a) $p = 0.1$ and (b) $p = 0.5$ for adding shortcuts. (c) Snapshots of log-income distributions for various p values at $t = 10^4$. The inset displays income-level segregation $\Delta\mu$ against p. Here we employ the WS network with $k = 4$, and $N = 10^3$, $\Delta\alpha = 10^{-3}$ in (a) and (b); $N = 10^4$, $\Delta\alpha = 5 \times 10^{-3}$ in (c). The other parameters are the same as Figs. 1(b) and 1(c).

In Fig. 3 we present the time evolution of g across various α configurations. For all cases, the dynamics exhibit three distinct regimes: (1) Normal diffusion, (2) Gaussian subdiffusion, and (3) non-Gaussian diffusion [see insets of Figs. 3(a) and 3(b)]. The transitions between these regimes occur at timescales $t_1 = [2Ja_0]^{1/(\lambda-1)}$ and $t_2 = [2Ja_0\Delta\alpha^2/\beta^2]^{1/(\lambda-2)}$, marking the crossovers from subdiffusion to normal diffusion and subsequently to ballistic or super-diffusive motion. These crossovers are highlighted by guidelines and shaded regions (see Sec. III D and Fig. S10 in SM [26] also for detailed derivations and numerical confirmations). Unlike the first two regimes, which are characteristic of the homogeneous BM model, the third regime is unique to the HBM model, arising specifically from configuration effects.

Along *Path 1*, ρ_+ and ρ_- overlap significantly, resulting in a single peak for the total distribution $\rho(x)$ [see Figs. 2(b) and 2(d)]. Consequently, g evolves on a single timescale, as described by Eq. (8), with inequality driven solely by diffusion. In this regime, g increases monotonically with $\mathcal{A}$ [see Fig. 3(a)]. Along *Path 2*, ρ_+ and ρ_- separate, leading to a bimodal $\rho(x)$ [see Figs. 2(c) and 2(e)]. Consequently, inequality is governed by both class division and diffusion. As indicated by Eq. (9), the substantial income gap between the two peaks contributes a baseline value of 0.5 to g. This manifests as a horizontal segment in the Lorenz curve, implying a kind of economic extinction of the poor class [see Figs. 3(c) and 3(d)]. The remaining contribution to g arises from diffusion within the rich class. We therefore analyze $\mathrm{Var}(X_{\mathrm{rich}})$, defined for incomes X_{rich} exceeding the median. In this case, decreasing $\mathcal{A}$ enhances $\mathrm{Var}(X_{\mathrm{rich}})$, driving the system toward a super-diffusive regime that accelerates condensation ($g \to 1$) [see Fig. 3(b) and Sec. III D in SM [26] for details]. Remarkably, introducing even modest heterogeneity and mixing within the 1D ring topology induces super-diffusive behavior, a phenomenon absent in the homogeneous BM model.

Finally, we investigate the effect of small-worldness [33] on income distributions in the HBM model (see Fig. 4 and Sec. IV, and Figs. S11–S13 in SM [26] for detailed numerical confirmations). We employ the Watts-Strogatz (WS) network, initializing the growth-rate configuration for the case of $\mathcal{A}_{\max}$ prior to rewiring with probability p. This rewiring process introduces heterogeneous links with probability $p/2$, thereby reducing assortativity such that $\mathcal{A} \simeq 1 - p$. Increasing p establishes shortcuts between spatially segregated regions with high and low growth rates. In contrast to the homogeneous BM model, small-world (SW) shortcuts in the HBM model disrupt not only long-range correlations but also regional income segregation, effectively dismantling log-income bimodality. As p increases, rich and poor clusters shrink, and long-range correlations decline [see Figs. 4(a) and 4(b)]. Moreover, regional income segregation weakens as poor (rich) clusters emerge within high (low) growth-rate regions. Consequently, the segregation of income levels $\Delta\mu$ decreases, and bimodality collapses as p rises [see Fig. 4(c) and Sec. IV in SM [26] for detailed numerical verification].

IV. SUMMARY AND REMARKS

To sum up, we investigated how regional growth-rate configurations affect income distributions. The emergence of bimodality, spatial correlations, and regional segregation—features consistent with global income patterns over the past half-century—can be linked to the absence of small-world connectivity in sparse regular networks, corresponding to small η (see Appendix A). We found that regional concentration of growth rates ($\mathcal{R}$) is associated with the development of bimodality and income-level segregation, whereas growth-rate assortativity ($\mathcal{A}$) influences the diffusive behavior and long-term inequality.

For Watts-Strogatz (WS) topologies, the introduction of small-world shortcuts connects high- and low-growth regions, which tends to reduce long-range correlations and weaken the bimodal structure of the income distribution. The reduced diffusion across growth-rate interfaces bears some similarity to localization effects induced by quenched disorder [34,35], while the resulting segregation of income levels is reminiscent of phase-separation-like behavior observed in nonequilibrium active matter systems [36,37].

Our model can be taken as a possible framework for interpreting aspects of the historical evolution of global inequality [20,21,38], particularly the first two of the three eras identified by Milanovic [12]. Sparse regular networks with large $\mathcal{R}$ are consistent with the first era, in which both within- and between-region inequalities increase. WS networks with small p, which exhibit stationary bimodal distributions, may be related to the second era, where global inequality and regional segregation become persistent. The third (contemporary) era, which does not show clear bimodality, has been associated with accelerated growth in developing economies such as China and India [12–14]. Incorporating temporal growth rates, $\alpha(t)$, would be a natural extension, it is beyond the scope of the present work. In addition, recent studies suggesting that trade and migration contribute to reducing global inequality [38,39] are qualitatively consistent with our results for WS networks with sufficiently large p.

A natural direction for future work is to consider continuous spectra of growth rates. While normally distributed growth rates have been studied in noninteracting [40] and mean-field limits [41], their behavior on complex networks

remains to be explored in more detail [42]. The role of heterogeneous volatility also remains an open question. Long-range correlations are not limited to income, but have been reported in other social indicators, such as housing prices [43] and voting patterns [44]. In systems with spatial heterogeneity in local conditions, including growth rates or infrastructure, the metrics $(\mathcal{A}, \mathcal{R})$ could serve as one possible measure to characterize configuration effects. Finally, capturing the full history of global income inequality may require extensions to temporal networks; in this context, the evolving structure of the world trade network [45,46] could offer additional insight.

ACKNOWLEDGMENTS

This research was supported by Basic Science Research Program through the National Research Foundation of Korea (NRF) (KR) [NRF-RS-2025-00514776 (J.H. and H.J.) and NRF-RS-2026-25489888 (J.H. and M.H.)].

DATA AVAILABILITY

The data that support the findings of this article are not publicly available. The data are available from the authors upon reasonable request.

APPENDIX A: HOMOGENEOUS BM MODEL ON SPARSE REGULAR NETWORKS

In general, the original Bouchaud and Mézard (BM) model [25] is represented by a stochastic differential equation (SDE):

$$dC_n = \alpha C_n dt + \beta C_n dW_{t,n} + \sum_{m(\neq n)} (J_{nm}C_m - J_{mn}C_n)dt, \quad \text{(A1)}$$

where n is an agent index, C_n is the income of node n, dt is a time interval, $W_{t,n}$ is the Wiener process of n at time t, α is the growth rate, β is the volatility and J_{nm} is the element of an interaction matrix $\mathbf{J}$, respectively. This follows the Itô interpretation.

To focus on the relative income of the nodes, we denote a normalized income $c \equiv C/\bar{C}$, where $\bar{C}$ is an average income. Then we can rewrite Eq. (A1) with the proper notation [47] as

$$dc_n = J \sum_{\{m|a_{nm}=1\}} \left(\frac{c_m}{k_m} - \frac{c_n}{k_n}\right)dt + \beta c_n dW_{t,n}, \quad \text{(A2)}$$

where a_{mn} is the element of the adjacency matrix $\mathbf{a}$ for an interaction network, and the strength of the interaction between node n and node m is $J_{nm} = J/k_m$ with $J > 0$, and the degree of node m is k_m. For the case of random networks, $J_{mn} = a_{mn}J/\langle k\rangle$ with the average degree $\langle k\rangle$. This rescaling of C and the normalization by division $\bar{C}$ do not alter Eq. (A1) nor the Gini index g and the Hellinger distance h. In our numerical simulation based on Eq. (A1), this process is identical to Eq. (A2), which also guaranties $\langle c\rangle = 1$. For a sufficiently dense (or small-world) network, $\rho(c,t)$ converges to the stationary distribution for large t, and most previous studies focus on it [48–55].

For a regular network, Eq. (A2) is reduced by

$$dc_n = J\left(\bar{c}_n^{(k)} - c_n\right)dt + \beta c_n dW_{t,n}, \quad \text{(A3)}$$

where $\bar{c}_n^{(k)}$ is the average normalized income over k neighbors of a node n. Equation (A3) is solved by the effective field theory (EFT) ansatz [54]

$$\bar{c}_n^{(k)} \to \theta(\eta)c_n^{1-\eta}, \quad \text{(A4)}$$

where a field exponent $\eta \in (0, 1]$ and a normalization factor $\theta(\eta)$ from $\langle c\rangle = 1$. The field exponent η displays the nonlinear effect of local interactions, approximated by c_n itself. Therefore, Eq. (A3) can be rewritten as

$$dc_n = J\left[\theta(\eta)c_n^{1-\eta} - c_n\right]dt + \beta c_n dW_{t,n}. \quad \text{(A5)}$$

The study by Ma *et al.* [54] demonstrates that η converges to a constant for sufficiently large $z \equiv k/N$ ($\geqslant 10^{-2}$) and $\rho(c)$ is the generalized inverse-gamma distribution.

However, for small z, $\eta(t)$ does not converge to a stationary solution. Hence, the temporal behavior of η should be analyzed in the sparse regular network. Let $x \equiv \ln c$ and assume that ηx is sufficiently small, then the first-order approximation of Eq. (A5) becomes a time-dependent *Ornstein-Uhlenbeck* (OU) process [56] as

$$dx_n = J\eta\theta(\eta)\left[\left(\frac{\theta(\eta)-1}{\eta\theta(\eta)}\right) - x_n\right]dt - \frac{\beta^2}{2}dt + \beta dW_{t,n}, \quad \text{(A6)}$$

where η and $\theta(\eta)$ depend on t.

Surprisingly, for large t, the variance of the process of Eq. (A6) is asymptotically similar to that of the ordinary OU process: $\sigma_t^2 = \beta^2/[2J\eta\theta(\eta)]$ [57], where both η and θ are substituted as constants. This phenomenon depends on the slow decay of $\eta(t)$ as $\rho(x,t) \approx \rho_{\text{eq}}^{(\text{OU})}(x,t;\eta_t,\theta_t)$. If Eq. (A4) is in good approximation, the random variables, $Y = \ln \bar{c}^{(k)}$ and $X = \ln c$, are in the linear relationship as $Y = (1-\eta)X + \ln\theta(\eta)$.

According to the least square linear regression: $1 - \eta = \text{Cov}(X,Y)/\text{Var}(X)$ (see Sec. I A and Figs. S1 and S2 in SM [26]), we empirically find that η follows the time-asymptotic power law as

$$\eta(t) \sim a_0 t^{-\lambda} \quad \text{for large } t, \quad \text{(A7)}$$

where a_0 is constant and $0 < \lambda \leqslant 1$ for small z, and $\theta(\eta) \to 1$. This supports our approximation that $\rho(x,t) \approx \rho_{\text{eq}}^{(\text{OU})}(x,t;\eta_t,\theta_t)$ at each point in time is approximately Gaussian. For large t, the variance $\sigma_t^2 = \beta^2 t^\lambda/(2Ja_0)$ and the mean $\mu_t = -\sigma_t^2/2$ of $\langle c\rangle = 1$, such that $c_t \sim \text{Lognormal}(\mu_t, \sigma_t^2)$.

For the one-dimensional (1D) ring topology under the small β condition, the SDE for X corresponds to the multidimensional OU process, and the interaction matrix is marginally stable [58]. Then η is given by

$$\eta(t) = \frac{1 - e^{-2Jt}I_0(2Jt)}{2Jte^{-2Jt}[I_0(2Jt) + I_1(2Jt)]}, \quad \text{(A8)}$$

where I_ℓ ($\ell = 0, 1, 2, \dots$) is the modified Bessel function of the first kind. This expression satisfies $a_0 t^{-1/2}$ for large t, and is also consistent with Eq. (A7). The power-law decay of η corresponds to the vanishing of nonlinearity in the effective field, which results in the convergence of income of neighboring nodes. On the other hand, the variance σ_t^2 increases over time t, so almost all income is condensed (localized) in narrow regions for large t, which corresponds to the localization in

the 1D stochastic heat equation or 1D Kardar-Parisi-Zhang equation as well.

The ℓ-ranged covariance is as

$$\mathrm{Cov}(X_n, X_{n+\ell}) = \beta^2 \int_0^t e^{-2Js} I_\ell(2Js) ds, \tag{A9}$$

for the same time t, the shorter the distance ℓ, the larger the covariance. The results in strong spatial correlations of X that make the clustering of rich and poor regions, as shown in Figs. 1(b) and 1(c), respectively [see Sec. I A in SM [26] for details of $\mathrm{Var}(X)$, $\mathrm{Cov}(X, Y)$, $\eta(t)$, and long-range correlations]. The BM model in a sparse regular network exhibits strong spatial correlations, while that in other network cases (the noninteractive case and the mean-field case) does not (see Fig. S3 in SM [26]) but log-income distributions are still unimodal. The log-normality of $\rho(c)$ for small z reported by Souma *et al.* [48], is derived with a time-dependent OU process of $x \equiv \ln c$. We show that it is valid only for small β and z.

In short, we develop a time-dependent EFT ansatz and derive temporal behaviors of statistical properties for the case of the 1D ring topology and the case of sparse regular networks by analytical and numerical methods.

APPENDIX B: GINI INDEX OF DECOUPLED DUAL LOG-NORMAL MIXTURE

For a single log-normal distribution $\mathrm{Lognormal}(\mu, \sigma^2)$, the Gini index g is given by

$$g = \mathrm{erf}(\sigma/2), \tag{B1}$$

which is also captured by the Lorenz curve $\mathcal{L}$ that is the cumulative sum of income fraction from the poorest to the richest sample. The $\mathcal{L}(f)$ divides the lower triangle into two regions. If upper and lower regions are denoted as A and B, respectively, g is given by

$$g \equiv \frac{A}{A+B} = 1 - 2B, \tag{B2}$$

where $A + B = 1/2$ and $B = \int_0^1 \mathcal{L}(f) df$.

When the log-income distribution is a mixture of two distributions, $\rho(x) = [\rho_1 + \rho_2]/2$, and is completely separable, i.e., support sets, X_1 and X_2, satisfy $X_2 \geqslant X_1$ ($h = 1$), the entire Lorenz curves $\mathcal{L}$ represented by $\mathcal{L}_1$ and $\mathcal{L}_2$, are rescaled Lorenz curves of ρ_1 and ρ_2, respectively.

If the total population (income) share of the first and second distributions is given by f_1 and f_2 (S_1 and S_2), then B is decomposed as (see Fig. 5)

$$B = B_1 + B_2 + (1 - f_1) S_1. \tag{B3}$$

Since the Lorenz curves, $\mathcal{L}_1$ and $\mathcal{L}_2$, for sufficiently large decoupling ($h \approx 1$) correspond to the rescaling of the single

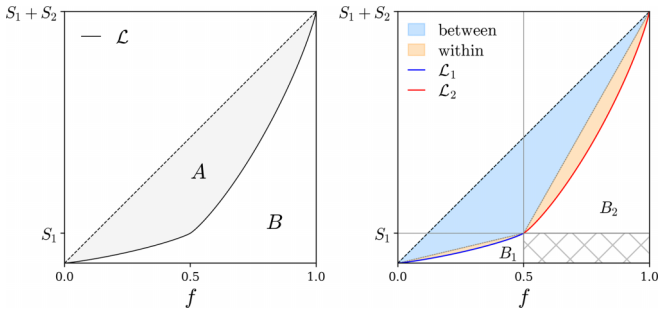

FIG. 5. Visualization of Lorenz curve and decomposition for the case of a dual log-normal mixture with large decoupling: Entire Lorenz curve $\mathcal{L}$ (left); Decomposition of $\mathcal{L}$ (right), where blue and red solid lines show rescaled Lorenz curves $\mathcal{L}_1$ and $\mathcal{L}_2$, and S_1 and S_2 represent total income share from each log-normal distribution. Light-blue and light-orange shadowed areas show contributions of between- and within-inequality on g for $f_1 = f_2 = 1/2$.

Lorenz curve of each distribution, the rescaled areas, B_1 and B_2, are rewritten as

$$B_1 = f_1 S_1 \tfrac{1}{2}(1 - g_1), \quad B_2 = f_2 S_2 \tfrac{1}{2}(1 - g_2), \tag{B4}$$

where g_1 and g_2 are the corresponding Gini indices for ρ_1 and ρ_2, respectively. Substituting $f_1 = f_2 = 1/2$, Eq. (B4) and Eq. (B3) into Eq. (B2), g is as

$$g = \tfrac{1}{2}(1 + S_1 g_1 + S_2 g_2) - S_1. \tag{B5}$$

This representation is valid for arbitrary ρ_1 and ρ_2 with $f_1 = f_2 = 1/2$ and $X_2 \geqslant X_1$. For the dual log-normal mixture of $\mathrm{Lognormal}(\mu_1, \sigma^2)$ and $\mathrm{Lognormal}(\mu_2, \sigma^2)$, where $\mu_1 < \mu_2$, $h \approx 1$, and the same fractions $f_1 = f_2 = 1/2$ (population shares for ρ_1 and ρ_2), the income shares S_1 and S_2 are approximately as

$$\begin{aligned} S_1 &= \frac{\langle c_1 \rangle}{\langle c_1 \rangle + \langle c_2 \rangle} = \frac{1}{1 + e^{\Delta\mu}}, \\ S_2 &= \frac{\langle c_2 \rangle}{\langle c_1 \rangle + \langle c_2 \rangle} = \frac{1}{1 + e^{-\Delta\mu}}, \end{aligned} \tag{B6}$$

where $\langle c_1 \rangle = \exp(\mu_1 + \sigma^2/2)$, $\langle c_2 \rangle = \exp(\mu_2 + \sigma^2/2)$ from the log-normal nature, and $\Delta\mu = (\mu_2 - \mu_1)$. Moreover, for the perfectly assortative case with $\mathcal{A}_{\max}$, $\mu_1 = \mu_t^-$, $\mu_2 = \mu_t^+$, $\sigma^2 = \sigma_t^2 = \beta^2 t^\lambda / (2J a_0)$, and $\Delta\mu = 2\Delta\alpha t$ for large t.

Substituting $f_1 = f_2 = 1/2$, Eq. (B6), and Eq. (B1) into Eq. (B5), $g(t)$ becomes

$$g(t) = \frac{1}{2}\left(1 - \frac{2}{1 + e^{-2\Delta\alpha t}}\right) + \frac{1}{2}\mathrm{erf}(\sigma_t/2), \tag{B7}$$

which corresponds to Eq. (9). For small decoupling $h \ll 1$, g of the dual log-normal mixture becomes more complicated (see Sec. III A in SM [26]).

[1] T. Piketty, *Capital in the Twenty-First Century* (Harvard University Press, Cambrige, 2014).

[2] R. Gibrat, *Les inégalités économiques*, Théses (Recueil Sirey, Paris, France, 1931).

[3] P. Pestieau and U. M. Possen, A model of wealth distribution, Econometrica **47**, 761 (1979).

[4] P. Pestieau and U. M. Possen, A model of income distribution, Eur. Econ. Rev. **17**, 279 (1982).

[5] D. Slottje, Modeling income distributions and Lorenz curves, J. Econ. Inequal. **8**, 525 (2010).

[6] B. K. Chakrabarti, A. Chakraborti, S. R. Chakravarty, and A. Chatterjee, *Econophysics of Income and Wealth Distributions* (Cambridge University Press, Cambridge, UK, 2013).

[7] M. Nirei and S. Aoki, Pareto distribution of income in neoclassical growth models, Rev. Econ. Dyn. **20**, 25 (2016).

[8] X. Gabaix, J.-M. Lasry, P.-L. Lions, and B. Moll, The dynamics of inequality, Econometrica **84**, 2071 (2016).

[9] T. Piketty and E. Saez, Income inequality in the united states, 1913–1998, Q. J. Econ. **118**, 1 (2003).

[10] F. Bourguignon and C. Morrisson, Inequality among world citizens: 1820–1992, Am. Econ. Rev. **92**, 727 (2002).

[11] B. Milanovic, Global inequality of opportunity: How much of our income is determined by where we live? Rev. Econ. Stat. **97**, 452 (2015).

[12] B. Milanovic, The three eras of global inequality, 1820–2020 with the focus on the past thirty years, World Dev. **177**, 106516 (2024).

[13] P. Liberati, The world distribution of income and its inequality, 1970–2009, Rev. Income Wealth **61**, 248 (2015).

[14] B. Milanovic, Global income inequality in numbers: In history and now, Global Policy **4**, 198 (2013).

[15] X. Sala-i-Martin, The world distribution of income: Falling poverty and ... convergence, period, Q. J. Econ. **121**, 351 (2006).

[16] M. Pinkovskiy and X. Sala-i Martin, Parametric estimations of the world distribution of income, Technical Report (National Bureau of Economic Research, 2009).

[17] S. Anand and P. Segal, What do we know about global income inequality? J. Econ. Lit. **46**, 57 (2008).

[18] J. L. Van Zanden, J. Baten, P. Foldvari, and B. Van Leeuwen, The changing shape of global inequality 1820–2000; exploring a new dataset, Rev. Income Wealth **60**, 279 (2014).

[19] C. Lakner and B. Milanovic, Global income distribution: From the fall of the berlin wall to the great recession, World Bank Econ. Rev. **30**, 203 (2016).

[20] M. Roser, Our World in Data (2017), https://ourworldindata.org/the-history-of-global-economic-inequality.

[21] L. Chancel, T. Piketty, E. Saez, and G. Zucman, *World Inequality Report 2022* (Harvard University Press, Cambridge, 2022).

[22] M. Roser, B. Rohenkohl, P. Arriagada, J. Hasell, H. Ritchie, and E. Ortiz-Ospina, Data page: World Bank income groups, https://ourworldindata.org/grapher/world-bank-income-groups (World Bank, Washington, DC, 2023), part of the publication "Economic Growth. Data adapted from World Bank.

[23] S. J. Rey and B. D. Montouri, US regional income convergence: A spatial econometric perspective, Region. Stud. **33**, 143 (1999).

[24] D. Yamamoto, Scales of regional income disparities in the USA, 1955–2003, J. Econ. Geo. **8**, 79 (2008).

[25] J.-P. Bouchaud and M. Mézard, Wealth condensation in a simple model of economy, Physica A **282**, 536 (2000).

[26] See Supplemental Material at http://link.aps.org/supplemental/10.1103/66j8-zpyg for more details, which includes Refs. [12,25,48,52,54,58,59].

[27] The value of the Pearson correlation coefficient is bounded between -1 and 1.

[28] M. Cinelli, L. Peel, A. Iovanella, and J.-C. Delvenne, Network constraints on the mixing patterns of binary node metadata, Phys. Rev. E **102**, 062310 (2020).

[29] Y. Kuramoto, Self-entrainment of a population of coupled nonlinear oscillators, Lect. Notes Phys. **39**, 420 (1975).

[30] E. Hellinger, Neue Begründung der Theorie quadratischer Formen von unendlichvielen Veränderlichen, J. reine angewandte Math. **1909**, 210 (1909).

[31] C. Gini, *Variabilità e mutabilità: Contributo allo studio delle distribuzioni e delle relazioni statistiche [Fasc. I.]*, Studi economico-giuridici pubblicati per cura della facoltá di Giurisprudenza della R. Universitá di Cagliari (Tipogr. di P. Cuppini, Bologna, Italy, 1912).

[32] For the BM model, $\rho(C)$ does not converge over time. However, for normalized income $c \equiv C/\bar{C}$, $\rho(c)$ converges over time such conditions that mean-field case and dense networks, and gives more mathematical conveniences. The log-normalized income is defined as $x \equiv \ln c$.

[33] Souma [48] has shown that in the BM model, the small-world effect changes wealth distribution from log-normal to power-law and eases inequality, resulting in a decrease of the Gini index.

[34] D. A. Abanin, E. Altman, I. Bloch, and M. Serbyn, *Colloquium:* Many-body localization, thermalization, and entanglement, Rev. Mod. Phys. **91**, 021001 (2019).

[35] R. Nandkishore and D. A. Huse, Many-body localization and thermalization in quantum statistical mechanics, Annu. Rev. Condens. Matter Phys. **6**, 15 (2015).

[36] M. E. Cates and J. Tailleur, Motility-induced phase separation, Annu. Rev. Condens. Matter Phys. **6**, 219 (2015).

[37] Y. Fily and M. C. Marchetti, Athermal phase separation of self-propelled particles with no alignment, Phys. Rev. Lett. **108**, 235702 (2012).

[38] A. Fink, IREF, https://en.irefeurope.org/publications/online-articles/article/reducing-global-inequality-growth-and-migration/ (2021).

[39] O. Hammar and D. Waldenström, Global earnings inequality, 1970–2018, Econ. J. **130**, 2526 (2020).

[40] A. Pluchino, A. E. Biondo, and A. Rapisarda, Talent versus luck: THE role of randomness in success and failure, Adv. Complex Syst. **21**, 1850014 (2018).

[41] M. Bernard, J.-P. Bouchaud, and P. L. Doussal, Mean-field theory for heterogeneous random growth with redistribution, Phys. Rev. E **113**, L032101 (2026).

[42] J. Hur, M. Ha, and H. Jeong, Interplay of network structure and talent configuration on wealth dynamics, Phys. Rev. E **110**, 024312 (2024).

[43] A.-C. Becharat, M. Benzaquen, and J.-P. Bouchaud, Diffusive nature of housing prices, Phys. Rev. Lett. **135**, 107401 (2025).

[44] J. Fernández-Gracia, K. Suchecki, J. J. Ramasco, M. San Miguel, and V. M. Eguíluz, Is the voter model a model for voters? Phys. Rev. Lett. **112**, 158701 (2014).

[45] M. Á. Serrano, M. Boguñá, and A. Vespignani, Patterns of dominant flows in the world trade web, J. Econ. Interact. Coord. **2**, 111 (2007).

[46] M.-Y. Cha, J. W. Lee, and D.-S. Lee, Patterns of international trades and nation's wealth, J. Korean Phys. Soc. **56**, 998 (2010).

[47] By using $\bar{C} = C(0)e^{\alpha t}$, we get $dc_n = d(C_n/\bar{C}) = dC_n/\bar{C} - (C/\bar{C}^2)d\bar{C} = dC_n/\bar{C} - \alpha c_n dt$ in Eq. (2).

[48] W. Souma, Y. Fujiwara, and H. Aoyama, Small-world effects in wealth distribution, arXiv:cond-mat/0108482.

[49] W. Souma, Y. Fujiwara, and H. Aoyama, in *Meeting the Challenge of Social Problems via Agent-Based Simulation: Post-Proceedings of the Second International Workshop on Agent-Based Approaches in Economic and Social Complex Systems* (Springer, 2003), pp. 37–49.

[50] D. Garlaschelli and M. I. Loffredo, Wealth dynamics on complex networks, Physica A **338**, 113 (2004).

[51] D. Garlaschelli and M. I. Loffredo, Effects of network topology on wealth distributions, J. Phys. A: Math. Theor. **41**, 224018 (2008).

[52] M. Medo, Breakdown of the mean-field approximation in a wealth distribution model, J. Stat. Mech. (2009) P02014.

[53] T. Ichinomiya, Power-law exponent of the Bouchaud-Mézard model on regular random networks, Phys. Rev. E **88**, 012819 (2013).

[54] T. Ma, J. G. Holden, and R. Serota, Distribution of wealth in a network model of the economy, Physica A **392**, 2434 (2013).

[55] T. Ichinomiya, Bouchaud-Mézard model on a random network, Phys. Rev. E **86**, 036111 (2012).

[56] C. W. Gardiner, *Handbook of Stochastic Methods: For Physics, Chemistry and the Natural Sciences*, Lecture Notes in Mathematics (Springer, Berlin/Heidelberg, Germany, 1990), Vol. 3.

[57] In the ordinary OU process, $\rho_{\rm eq}^{(\rm OU)}(x)$ is a Gaussian with variance σ^2 that converges to the ratio of the diffusion coefficient to the dissipation factor, $\sigma^2 \to \beta^2/[2J\eta\theta(\eta)]$.

[58] J.-P. Bouchaud, The self-organized criticality paradigm in economics & finance, arXiv:2407.10284.

[59] K. I. Park, M. Park, *et al.*, *Fundamentals of Probability and Stochastic Processes with Applications to Communications* (Springer, New York, 2018).